Research article

Alexander Bommer and Christoph Becher*

New insights into nonclassical light emission from defects in multi-layer hexagonal boron nitride

https://doi.org/10.1515/nanoph-2019-0123
Received April 24, 2019; revised June 19, 2019; accepted June 21, 2019

Abstract: In recent years, mono-layers and multi-layers of hexagonal boron nitride (hBN) have been demonstrated as host materials for localized atomic defects that can be used as emitters for ultra-bright, non-classical light. The origin of the emission, however, is still subject to debate. Based on measurements of photon statistics, lifetime and polarization on selected emitters, we find that these atomic defects do not act as pure single photon emitters. Our results strongly and consistently indicate that each zero phonon line of individual emitters comprises two independent electronic transitions. These results give new insights into the nature of the observed emission and hint at a double defect nature of emitters in multi-layer hBN.

Keywords: hexagonal boron nitride; single photon emitters.

PACS: 42.50.Ar; 78.55.-m; 78.67.-n.

1 Introduction

Recently, two-dimensional van der Waals materials have emerged as promising platforms for optoelectronics [1–3], candidates for future UV-LEDs [4, 5] and host materials for emitters of non-classical light [6–15]. Especially atomic defects in hexagonal boron nitride (hBN) have been shown to belong to the brightest emitters of non-classical light ever reported. hBN is a semiconductor with a large band gap of around 6 eV [16]. Therefore, it is widely believed that at the origin of the emission are localized defects in the host material that give rise to electronic transitions between discrete energy levels within the band gap, as it is the case for color centers in diamond [17, 18]. However, the exact nature of the defects still remains unclear and is the subject of ongoing experimental and theoretical investigations [19–22]. For application in quantum information one needs narrowband and background free emission lines. The emitters selected in this work fulfill these criteria and exhibit spectra consisting of an asymmetric zero phonon line (ZPL) and a phonon side band approximately 165 meV red shifted from the ZPL. This energy shift corresponds to a well-known phonon mode in hBN [23–25]. The asymmetry of the ZPL is commonly attributed to phonon interaction, and the ZPL wavelengths have been shown to spread across a range from 500 to 800 nm [26], which is attributed to strain inside the host crystal [9, 27]. Independent of the emission wavelength, the ZPL is assumed to consist of a single, linearly polarized dipole transition giving rise to single photon emission. In this publication, on the contrary, we provide strong evidence for the presence of two independent emitters in each defect and show that the second line causing the asymmetry of the ZPL indeed is a second electronic transition. By carefully evaluating photon correlation measurements, we see that we only are able to fully reproduce our data by using an extended $g^{(2)}$-function that takes into account two independent transitions. We gain full access to the parameters of the $g^{(2)}$-function via independently measuring the spectra and the excitation power-dependent photon emission rates of the corresponding emitters. We further confirm the existence of double defects via measuring polarization-dependent spectra and performing time-correlated single photon counting (TCSPC) measurements.

2 Investigation of single photon emission from point defects in hBN

We spectroscopically investigate micrometer sized multi-layer flakes of hBN in a home-built laser scanning confocal microscope under continuous wave excitation at $\lambda = 532$ nm. Experiments are performed at room temperature if not indicated otherwise. The commercially

*Corresponding author: Christoph Becher, Universität des Saarlandes, Fachrichtung Physik, Campus E2.6, 66123 Saarbrücken, Germany, e-mail: christoph.becher@physik.uni-saarland.de.
https://orcid.org/0000-0003-4645-6882
Alexander Bommer: Universität des Saarlandes, Fachrichtung Physik, Campus E2.6, 66123 Saarbrücken, Germany

available flakes (Graphene Supermarket, Graphene Laboratories Inc., Ronkonkoma, NY, USA) are diluted in a solution (50% water, 50% ethanol) with a concentration of 5.5 mg/ml and put in an ultrasonic bath to break up agglomerates. The solution is drop cast (5–10 µl) onto a silicon wafer with an iridium layer for enhanced photon collection efficiency. The substrate is heated on a hotplate to 70°C to evaporate the liquid. After drop casting, individual flakes can be examined in the confocal microscope.

Figure 1A, D and G show typical spectra of point emitters inside the flakes. Although they differ in their central wavelengths, their spectral shapes are very similar. The spectra are fit with four Lorentzian lines which we will discuss later in closer detail. Saturation measurements in Figure 1B, E and H show typical saturation count rates (≈1–2 Mcts/s) and saturation powers (≈1 mW) of these emitters, in good agreement to previous reports [8–10]. The red lines are fits according to

$$I(P) = \frac{I_{\text{sat}} \cdot P}{P_{\text{sat}} + P} + C_{\text{back}} \cdot P. \tag{1}$$

Here, I_{sat} and P_{sat} are the saturation count rates and saturation powers of the emitters, whereas C_{back} describes a potential contribution due to linear background emission stemming from the host material. Note that this contribution is negligible in the presented data. This is in accordance with the very clean spectra presented in Figure 1A, D and G, where also no significant background contribution is visible. In approximately one out of 50 flakes

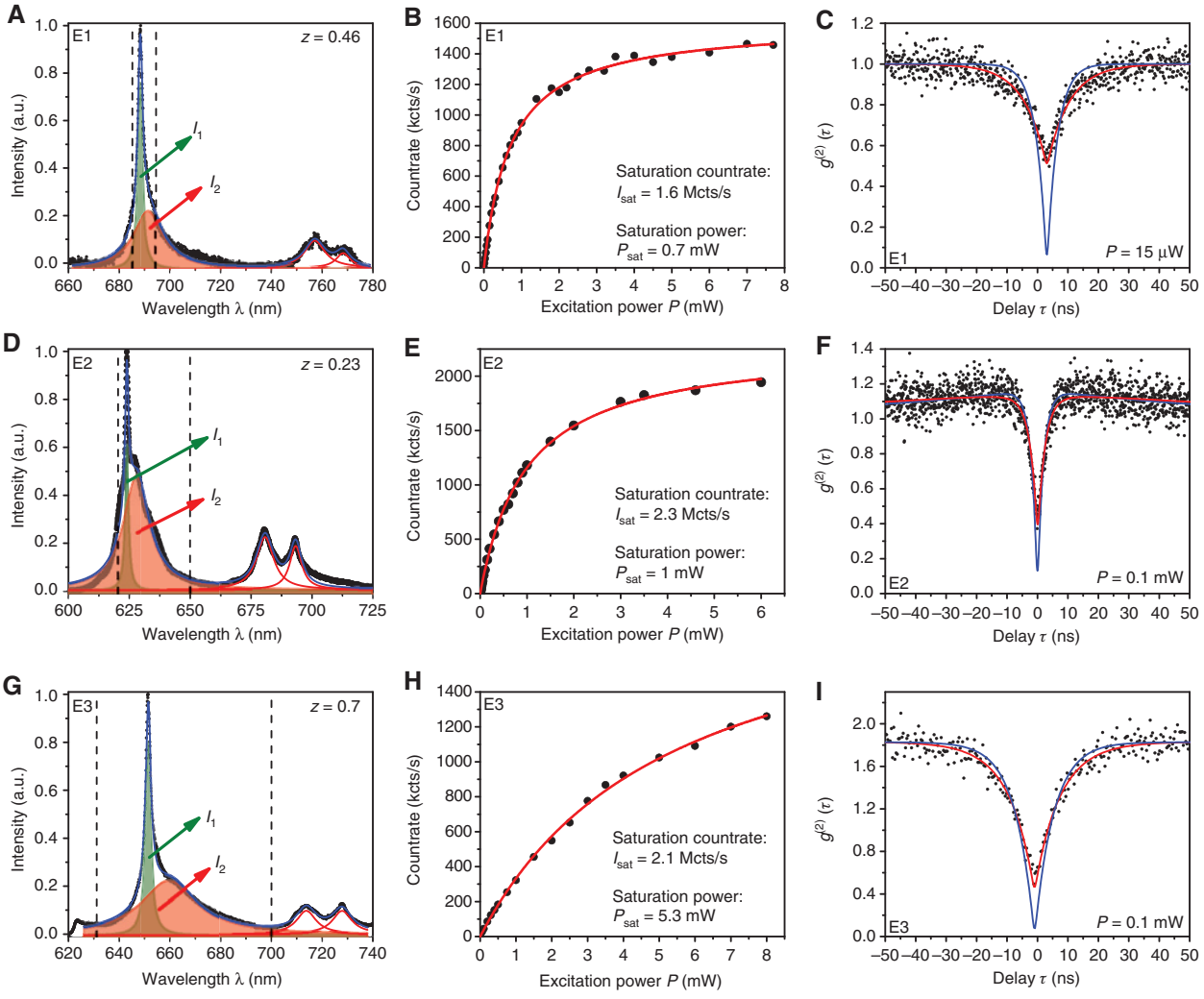

Figure 1: Photoluminescence spectra and single photon emission from individual defects in hBN.
(A, D, G) Typical spectra of three defects (E1, E2 and E3) in hBN consisting of four Lorentzian lines; (B, E, F) Saturation measurements on the defects from A, D and G with no significant background contribution; (C, F, I) $g^{(2)}$-intensity correlation measurements on the defects shown in A, D and G. Photons are collected from the spectral regions enclosed in dashed lines in A, D and G, respectively. See main text for details.

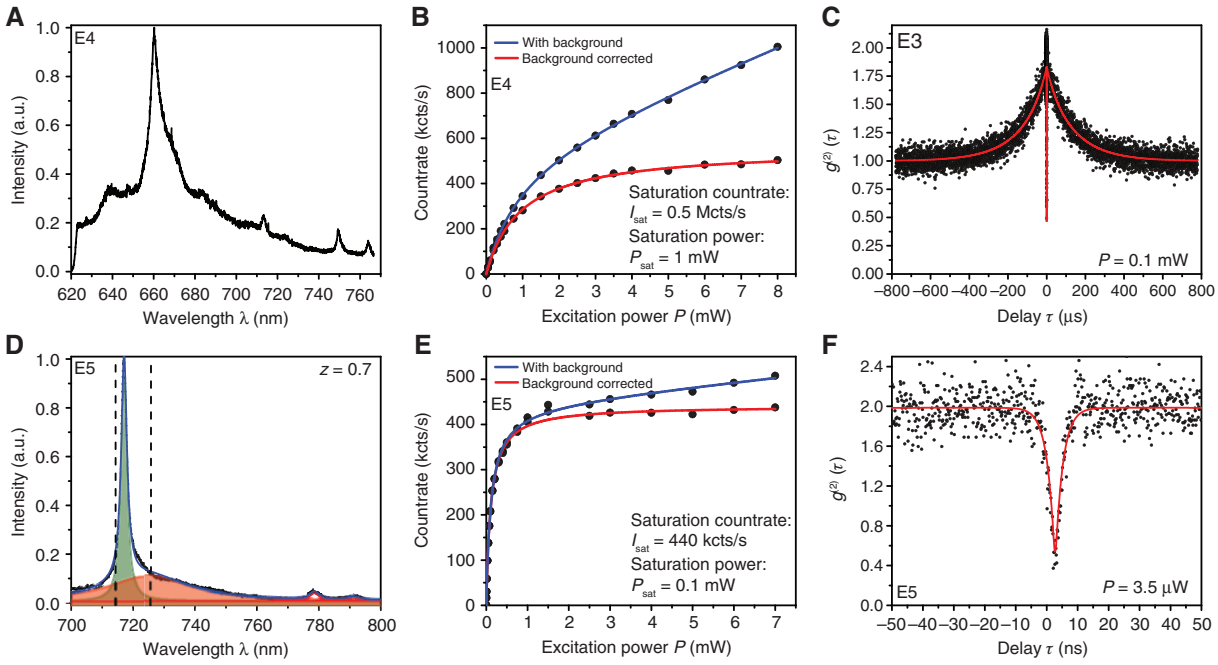

Figure 2: Photoluminescence spectra and single photon emission from individual defects in hBN with strong and vanishing background emission, respectively.
(A) Spectrum of an emitter in hBN (E4) with a clear background contribution. (B) Saturation measurement on the emitter in A. The background contribution is visible as prominent linear increase in the emission rate at increasing excitation powers. (C) $g^{(2)}$-function on an hBN emitter (E3) showing typical bunching timescales of several hundreds of microseconds. (D, E, F) Spectrum, saturation measurement and $g^{(2)}$-function of an emitter (E5) with a clean spectrum. Background contribution becomes relevant at about $20\times P_{sat}$. Still, $g^{(2)}(0)$ is strongly limited even at almost vanishing excitation powers.

background-free emission can be found. Contrary to these findings, Figure 2A) shows a spectrum, which clearly contains additional background emission. This background emission is also visible as a prominent linear increase in a corresponding saturation measurement in Figure 2B. Note that the saturation measurements are always taken by integrating the emission intensity over the ZPL and the two sidebands (cf. the four Lorentzian lines in Figure 1).

As a last step, we perform $g^{(2)}$-photon correlation measurements (Figure 1C, F and I to get information about the photon statistics. In order to reduce the potential influence of background emission (although not present in the current experiments) on the photon statistics measurements, we restrict the spectral window from which we collect photons for the $g^{(2)}$-measurements to the region of the ZPL (regions enclosed by dashed lines in the corresponding spectra) and take the measurements at excitation powers far lower than the emitters' saturation powers. Despite vanishing background fluorescence, the $g^{(2)}$-functions do not vanish at all at zero time delay as one would expect for an ideal single photon source. Figure 2D–F further shows an example, where background emission from the host material is present but becomes relevant only at about $20\times P_{sat}$. Nevertheless, for almost vanishing excitation power ($P=3.5$ μW), the value of $g^{(2)}(0)$ is still much larger than zero. As we show below also the timing jitter of the photon detectors does not explain the deviation from ideal single photon statistics as the emitter fluorescence lifetime is larger than the jitter. Instead, we have to assume that the asymmetric shape of the ZPL is due to the presence of two independent emission lines.

In the following we develop a model for the photon correlation functions that, besides background emission and the timing jitter of the photon detector, accounts for the presence of a second emitter and prove that this model fully reproduces the measurements. We start with the well-known $g^{(2)}$-function for a three-level system:

$$g_i^{(2)}(\tau)=1-(1+a)\cdot e^{-\frac{|\tau|}{\tau_1}}+a\cdot e^{-\frac{|\tau|}{\tau_2}} \tag{2}$$

We now, step by step, include all experimental parameters that influence the shape of the $g^{(2)}$-function: Although negligible in the presented data (but not in general), we start with uncorrelated background emission, that can be extracted from saturation measurements. Including this into the model, the $g^{(2)}$-function reads [28]

$$g_p^{(2)}(\tau) = \frac{1}{p^2} \cdot [g_i^{(2)}(\tau) - (1-p^2)] \tag{3}$$

Here, p is the fraction of measured photons stemming from the emitter compared to the measured total count rate. Note, that one should also consider dark counts of the detector in the description. In our case, these dark counts (≈100–200 cts/s) are negligible compared to the signal from the emitters. Second, we include the timing jitter σ of the counting electronics. This jitter is an uncertainty in the time between the arrival and the detection of a single photon and has been measured via ultra-fast laser pulses (σ≈490 ps). It is included via the convolution of Eq. (3) with the Gaussian shape of the instrument response function IRF(t).

$$g_{p,j}^{(2)}(\tau) = \mathrm{IRF}(\tau) * g_p^{(2)}(\tau) = \int_{-\infty}^{\infty} \mathrm{IRF}(\tau) \cdot g_p^{(2)}(\tau - t)dt \tag{4}$$

Equation (4) is the final description for the case that we collect emission from exactly one single emitter. The blue solid lines in Figure 1C, F and I are fits to the data according to this model. It strikes the eye that this function is not able to reproduce the data. In particular, the model demands a much lower value for $g^{(2)}(0)$ than it is provided by the data. We want to stress that we also can reproduce the data by taking the signal to background ratio p as a fit parameter. This, however, strongly contradicts our findings of vanishing background in the spectrum and the saturation measurement.

Therefore, as a last step, we also take into account the influence of a second emitter in the detection focal volume. Let $I_{\mathrm{tot}} = I_1 + I_2$ be the total detected emission with $I_1 = z \cdot I_{\mathrm{tot}}$ and $I_2 = (1–z) \cdot I_{\mathrm{tot}}$ being the relative fractions of the emission of emitter 1 and emitter 2, respectively. This leads to

$$g^{(2)}(\tau) = \frac{\langle I_{\mathrm{tot}}(t) I_{\mathrm{tot}}(t+\tau)\rangle}{\langle I_{\mathrm{tot}}(t)\rangle^2}$$
$$= z^2 \cdot g_1^{(2)}(\tau) + (1-z)^2 \cdot g_2^{(2)}(\tau) + \underbrace{\frac{\langle I_2(t) I_1(t+\tau)\rangle}{\langle I_{\mathrm{ges}}(t)\rangle^2} + \frac{\langle I_1(t) I_2(t+\tau)\rangle}{\langle I_{\mathrm{ges}}(t)\rangle^2}}_{g_{\mathrm{mix}}^{(2)}}.$$

In order to reduce the number of fit parameters, we assume $g_1^{(2)}(\tau) = g_2^{(2)}(\tau)$. Because of the independence of I_1 and I_2, the two mixing terms will be constant for all τ and by making the assumption that $g_1^{(2)}(0) = g_2^{(2)}(0) = 0$ (corresponding to the observed vanishing background), we find $g_{\mathrm{mix}}^{(2)} = 2z(1-z)$. We eventually arrive at

$$g^{(2)}(\tau) = (1 - 2z(1-z)) g_{p,j}^{(2)}(\tau) + 2z(1-z). \tag{5}$$

In contrast to reports in literature, where the asymmetry of the ZPL is attributed to phonon interaction [8], we here fully reproduce the lineshape by fitting two Lorentzian lines representing two independent electronic transitions. By calculating the areas under the individual Lorentzians, we get information about the relative oscillator strengths of both emitters, corresponding to the parameter z in Eq. (5) (numbers also given in the spectra in Figures 1 and 2). By taking into account the double emission spectrum within the model (Eq. (5)) for the $g^{(2)}$-function, we are able to perfectly describe the measured photon correlation data (solid red lines in Figures 1C, F, I and 2C and F).

Interestingly, our photon correlation measurements correspond perfectly to reports in literature in terms of bunching dynamics and dips in the $g^{(2)}$-function at zero time delay [8–10]. Non-vanishing values of $g^{(2)}(0)$ in these reports were always attributed to residual background fluorescence which, however, is not further defined or shown. To our knowledge, the full set of information needed to accurately describe the situation has never been reported [8, 10, 29, 30]. Furthermore, we want to point out that most of the emitters measured in this work show very strong bunching on a timescale of several hundreds of microseconds up to milliseconds as it has been shown in previous work (see, for example, Figure 2C) [9, 10]. Therefore, a proper normalization of the $g^{(2)}$-function to the constant number of events for long time delays τ or to the recorded photon count rates is imperative. The absence of satisfactorily explanations in literature and the excellent agreement of measured photon correlation functions with the double defect model suggest that most probably the majority of *single* emitters in literature are indeed double defects.

3 Spectroscopic evidence for double defects

We now turn in closer detail to the emitters optical spectra providing further evidence for our model. Figure 3 shows a typical photoluminescence spectrum of a defect in hBN at room temperature and at a temperature of 5 K. For the low-temperature experiments the sample was mounted in a helium-flow cryostat. In analogy to the defects discussed in Section 2 the room temperature ZPL can be fit by the sum of two Lorentzian lines. The different widths of the two Lorentzians (also apparent in the spectra of Figures 1 and 2) are potentially a result of different electron-phonon coupling, e.g. due to a different symmetry or orientation of defects in the lattice resulting in coupling to a different

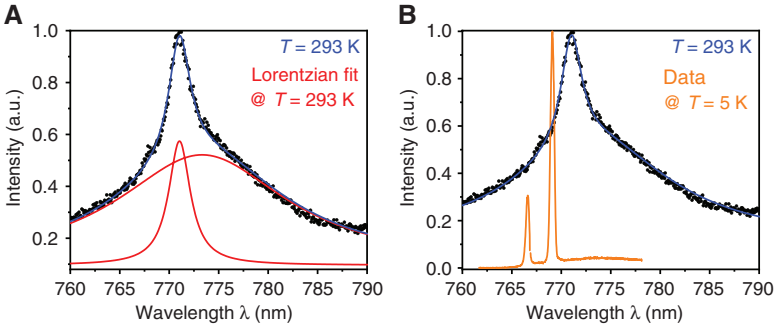

Figure 3: Photoluminescence spectrum of a typical emitter in hBN at room and cryogenic temperatures.
The black dots and blue lines are measured data and bi-Lorentzian fits to the data, respectively, at room temperature. The two red lines in (A) represent the individual Lorentzians of the bi-Lorentzian fit. The orange curve in (B) corresponds to the emission spectrum at 5 K.

subset of lattice phonons. Upon cooling to 5 K, these two lines shift to shorter wavelengths, their width strongly narrows and the lines become clearly distinguishable in the emission spectrum. This is clear evidence that the photoluminescence spectrum of this emitter indeed consists of two spectral lines. The emission lines at 5 K show a Gaussian line shape with similar widths (full width at half maximum) of 202 GHz and 222 GHz, respectively. The Gaussian line shapes indicate an inhomogeneous broadening mechanism such as spectral diffusion. In the following we discuss further spectroscopic features that support the double defect model.

Figure 4 shows normalized emission spectra of a collection of emitters in the multi-layer flakes under investigation. The central wavelength λ_1 of the highest energy line (line 1) ranges from 600 to 720 nm. This wavelength range is limited by the spectral filter window in which we collect fluorescence. On the ordinate axis the energy separations between all lines are shown, where the energy of line 1 (black) is always set to zero. It is apparent from Figure 4 that the energy distances between the lines remain approximately constant independent of the central wavelength of line 1 in the spectrum. In literature, the spectrum is described as an asymmetric ZPL with a red shifted (169.5 meV) phonon side band the energy of which belongs to a well-known transverse optical (TO) phonon mode in hBN [23–25]. We here first state that there are actually two ZPLs (line 1, black, and line 2, red) with two phonon side bands (line 3, blue, and line 4, orange). Averaged over all observed emitters with this particular spectral fingerprint, the energy difference between line 1 (black) and line 3 (blue) amounts to $\Delta E_{13} = 158$ (17) meV, whereas the distance between line 2 (red) and line 4 (orange) yields $\Delta E_{24} = 174$ (15) meV. Within the error bars, both values match the phonon mode at 169.5 meV. Staying in our picture of line 1 and 2 being electronic transitions, we thus attribute the lines 3 and 4 to be their respective phonon side bands. Note that an alternative interpretation of the results is possible: peaks 3 and 4 could originate from a coupling of the dominant ZPL line (line 1) to both the TO phonon mode at 169.5 meV and the longitudinal optical (LO) phonon mode at 199.6 meV. For the LO phonon mode, however, the electron-phonon scattering should be strongly reduced due to the cutoff of the phonon density of states close to this energy [24].

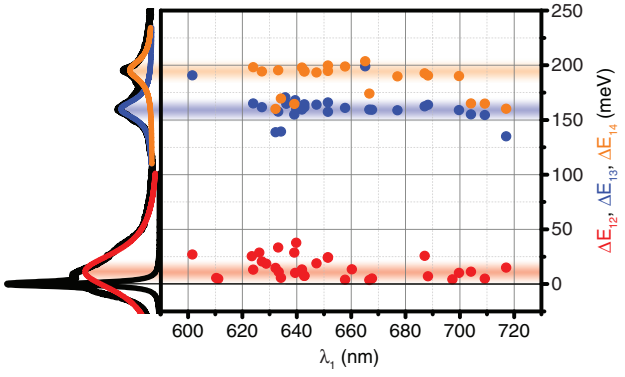

Figure 4: Spectral line position data extracted from 30 emitters that show comparable spectral fingerprints as explained in the main text.
Due to strain in the material, the central wavelengths of peak 1 range from 600 nm to 720 nm. However, independent of the wavelengths, the energy distance between the lines roughly remain constant. $\Delta E_{12} = 12$ (10) meV, $\Delta E_{13} = 158$ (17) meV, $\Delta E_{14} = 187$ (15) meV, $\Delta E_{24} = 174$ (15) meV. The semi-transparent, horizontal lines are a guide to the eye.

Next, we perform TCSPC measurements to gain further information about the lifetimes of the excited states of the investigated emitters. Two electronic transitions with potentially differing lifetimes should be visible as a bi-exponential decay. For the TCSPC measurements we use a white light laser filtered to 532 nm, with a pulse

duration of 200 ps and a pulse repetition rate of 10 MHz. Measurements on two typical hBN emitters (Figure 5A and C) are shown in Figure 5B and D (black dots). The solid lines are fits according to

$$L(t) = y_0 + \left(1 - \mathrm{erf}\left(-\frac{t-t_0}{\sigma}\right)\right) \cdot \sum_{i=1}^{n} A_i \cdot \mathrm{e}^{-\frac{t-t_0}{t_i}} \tag{6}$$

with one (blue, $n=1$) and two (red, $n=2$) time constants. As for the $g^{(2)}$-functions the instrument response function IRF(t) with a timing jitter of $\sigma = 490$ ps is included into the fit function via convoluting the Gaussian IRF(t) with the exponential decay of the electronic transition. In both measurements, the data points clearly follow a bi-exponential decay. The observed time constants ($t_1 = 0.82$ ns, $t_2 = 4.0$ ns and $t_1 = 1.7$ ns, $t_2 = 4.5$ ns) are compatible to time constants extracted from photon correlation measurements as in Section 2 and correspond to the range of typical lifetimes observed for this type of emitters [8–10]. In literature, however, usually just a single exponential decay is used to fit the data in a regime between 2 and 10 ns, and the full information about the timing resolution of the setup is not considered. The presence of two time constants of the same order of magnitude further indicates the existence of two excited states in the defect and corresponds perfectly with the assumption of two independent emitters in the same defect.

As a last step we now turn to the polarization of the defect emission. Linear excitation dipoles with visibilities between 20% and 80% have been reported, whereas the emission dipoles are supposed to show close to unity visibility and are linearly polarized [8, 15]. There is, however, a difference in the relative orientations of the excitation and emission dipoles between 30° and 90° [15, 30]. However, to our knowledge, polarization-dependent spectra have not been investigated in literature yet. Figure 5E and F show normalized emission spectra of two different hBN emitters with ZPL (line 1) at around 790 nm and 650 nm where different curves correspond to different settings of the polarization analyzer in the detection path. One can clearly see that dependent on the angle of a linear polarizer in the detection path, the line shape of the dominant line in the spectrum strongly varies. This indicates that here the two dipoles contributing to the ZPL have different relative polarizations. Note that we also can find spectra in which the line shape does not change significantly upon changing the detection angle of the polarization analyzer.

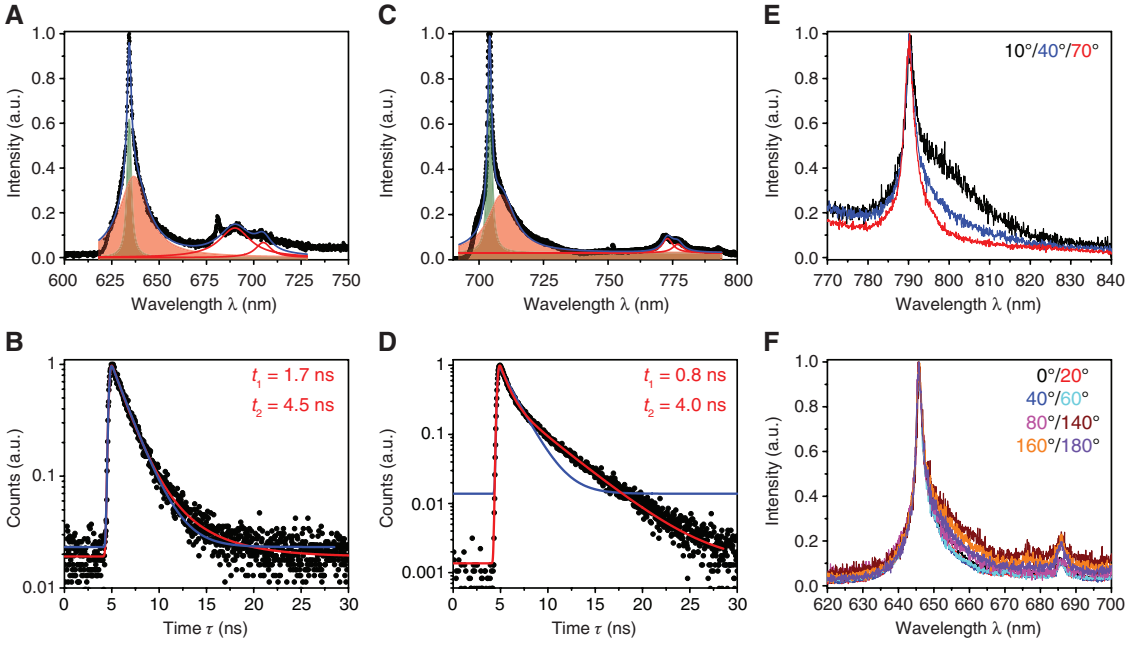

Figure 5: Photoluminescence spectra, fluorescence lifetime measurements and polarization-dependent emission from individual defects in hBN.

(A, C) Spectra of two typical emitters in hBN. The solid, colored lines are Lorentzian fits to the data. (B, D) Lifetime measurements on the emitters shown in A and C. The solid lines are fits according to a mono-exponential (blue) and bi-exponential (red) decay including the instrument response function of the setup. Both measurements follow a bi-exponential decay with time constants $t_1 = 0.82$ ns, $t_2 = 4.0$ ns and $t_1 = 1.7$ ns, $t_2 = 4.5$ ns. (E, F) Polarization-dependent optical spectra of two typical hBN emitters in emission. The line shape strongly depends on the angle of a polarizer in the detection path.

4 Conclusions

In summary, we presented new insights into the nature of non-classical light emission from defects in multi-layer flakes of hBN. Via careful evaluation of $g^{(2)}$-photon correlation measurements, TCSPC measurements and polarization-dependent emission spectra, we gather strong evidence that, in contrast to previous reports, these atomic defects are no single emitter systems but comprise two independent emitting systems here coined as "double defect". We draw this conclusion via collecting all necessary information to describe the photon statistics through independent measurements of the background contribution, the timing jitter of the counting electronic and the spectra of the emitters. Interestingly, our photon correlation measurements correspond perfectly to reports in literature in terms of bunching dynamics and dips in the $g^{(2)}$-function at zero time delay.

Our assumptions are corroborated by the decomposition of the asymmetric ZPL into two Lorentzian lines, both describing one individual electronic transition. Based on the existence of a characteristic phonon mode of hBN at 169.5 meV, we were able to assign the two dominant lines in the phonon side band to each of the electronic transitions. Eventually, the presence of a bi-exponential decay in TCSPC measurements and polarization-dependent emission spectra further support our model. We want to point out that our measured photon correlation functions perfectly correspond to the ones previously reported in literature. Based on these results we have to assume that many of the reported single photon emitters consist of "double defects" as described in this publication.

Acknowledgments: The authors want to thank Johannes Görlitz, Benjamin Kambs, Dennis Herrmann, Igor Aharonovich, Dirk Englund, Lee Bassett, Mike Ford and Adam Gali for helpful discussions. This work was partially funded by the European Union 7th Framework Program, FP7 Information and Communication Technologies under Grant Agreement No. 61807 (WASPS), Funder Id: http://dx.doi.org/10.13039/100011273.

References

[1] Srivastava A, Sidler M, Allain AV, Lembke DS, Kis A, Imamoglu A. Optically active quantum dots in monolayer WSe2. Nat Nanotechnol 2015;10:491–6.
[2] Palacios-Berraquero C, Barbone M, Kara DM, et al. Atomically thin quantum light-emitting diodes. Nat Commun 2016;7:12978.
[3] Chakraborty C, Kinnischtzke L, Goodfellow KM, Beams R, Vamivakas AN. Voltage-controlled quantum light from an atomically thin semiconductor. Nat Nanotechnol 2015;10:507–11.
[4] Kenji W, Takashi T. Hexagonal boron nitride as a new ultraviolet luminescent material and its application. Int J Appl Ceram Tech 2011;8:977–89.
[5] Watanabe K, Taniguchi T, Niiyama T, Miya K, Taniguchi M. Far-ultraviolet plane-emission handheld device based on hexagonal boron nitride. Nat Photonics 2009;3:591–4.
[6] Tonndorf P, Schmidt R, Schneider R, et al. Single-photon emission from localized excitons in an atomically thin semiconductor. Optica 2015;2:347–52.
[7] Koperski M, Nogajewski K, Arora A, et al. Single photon emitters in exfoliated WSe_2 structures. Nat Nanotechnol 2015;10:503–6.
[8] Tran TT, Bray K, Ford MJ, Toth M, Aharonovich I. Quantum emission from hexagonal boron nitride monolayers. Nat Nanotechnol 2016;11:37–41.
[9] Tran TT, Elbadawi C, Totonjian D, et al. Robust multicolor single photon emission from point defects in hexagonal boron nitride. ACS Nano 2016;10:7331–8.
[10] Tran TT, Zachreson C, Berhane AM, et al. Quantum emission from defects in single-crystalline hexagonal boron nitride. Phys Rev Appl 2016;5:034005.
[11] Martnez LJ, Pelini T, Waselowski V, et al. Efficient single photon emission from a high-purity hexagonal boron nitride crystal. Phys Rev B 2016;94:121405.
[12] Chejanovsky N, Rezai M, Paolucci F, et al. Structural attributes and photodynamics of visible spectrum quantum emitters in hexagonal boron nitride. Nano Lett 2016;16:7037–45.
[13] Schell AW, Tran TT, Takashima H, Takeuchi S, Aharonovich I. Non-linear excitation of quantum emitters in hexagonal boron nitride multilayers. APL Photonics 2016;1:091302.
[14] Jungwirth NR, Calderon B, Ji Y, Spencer MG, Flatte ME, Fuchs GD. Temperature dependence of wavelength selectable zero-phonon emission from single defects in hexagonal boron nitride. Nano Lett 2016;16:6052–7.
[15] Exarhos AL, Hopper DA, Grote RR, Alkauskas A, Bassett LC. Optical signatures of quantum emitters in suspended hexagonal boron nitride. ACS Nano 2017;11:3328–36.
[16] Cassabois G, Valvin P, Gil B. Hexagonal boron nitride is an indirect bandgap semiconductor. Nat Photonics 2016;10:262–6.
[17] Doherty MW, Manson NB, Delaney P, Jelezko F, Wrachtrup J, Hollenberg LC. The nitrogen-vacancy colour centre in diamond. Phys Rep 2013;528:1–46.
[18] Neu E, Steinmetz D, Riedrich-Möller J, et al. Single photon emission from silicon-vacancy colour centres in chemical vapour deposition nano-diamonds on iridium. New J Phys 2011;13:025012.
[19] Tawfik SA, Ali S, Fronzi M, et al. First-principles investigation of quantum emission from hBN defects. Nanoscale 2017;9:13575.
[20] Abdi M, Chou J-P, Gali A, Plenio MB. Color centers in hexagonal boron nitride monolayers: a group theory and ab initio analysis. ACS Photonics 2018;5:1967–76.
[21] Sajid A, Reimers JR, Ford MJ. Defect states in hexagonal boron nitride: assignments of observed properties and prediction of properties relevant to quantum computation. Phys Rev B 2018;97:064101.
[22] Lopez-Morales GI, Proscia NV, Lopez GE, Meriles CA, Menon VM. Toward the identification of atomic defects in hexagonal boron nitride: X-ray photoelectron spectroscopy and first-principles calculations. arXiv:1811.05924.

[23] Geick R, Perry CH, Rupprecht G. Normal modes in hexagonal boron nitride. Phys Rev 1966;146:543–7.
[24] Reich S, Ferrari AC, Arenal R, Loiseau A, Bello I, Robertson J. Resonant Raman scattering in cubic and hexagonal boron nitride. Phys Rev B 2005;71:205201.
[25] Nemanich RJ, Solin SA, Martin RM. Light scattering study of boron nitride microcrystals. Phys Rev B 1981;23:6348.
[26] Dietrich A, Bürk M, Steiger ES, et al. Observation of Fourier transform limited lines in hexagonal boron nitride. Phys Rev B 2018;98:081414.
[27] Grosso G, Moon H, Lienhard B, et al. Tunable and high-purity room temperature single-photon emission from atomic defects in hexagonal boron nitride. Nat Commun 2017; 8:705.
[28] Brouri R, Beveratos A, Poizat J-P, Grangier P. Single-photon generation by pulsed excitation of a single dipole. Phys Rev A 2000;62:063817.
[29] Mendelson N, Xu Z-Q, Tran TT, et al. Engineering and tuning of quantum emitters in few-layer hexagonal boron nitride. ACS Nano 2019;13:3132–40.
[30] Choi S, Tran TT, Elbadawi C, et al. Engineering and localization of quantum emitters in large hexagonal boron nitride layers. ACS Appl Mater Interfaces 2016;8: 29642–8.